INTERNATIONAL JOURNAL FOR NUMERICAL METHODS IN FLUIDS
Int. J. Numer. Meth. Fluids 2004; **44**:1017–1044 (DOI: 10.1002/fld.691)

LES of turbulent heat transfer: proper convection numerical schemes for temperature transport

A. Châtelain[1,2,*,†], F. Ducros[1,‡] and O. Métais

[1]*CEA Grenoble, 17, rue des Martyrs, 38054 Grenoble Cedex 9, France*
[2]*LEGI, Institut National Polytechnique de Grenoble, BP 53-38041 Grenoble Cedex 9, France*

SUMMARY

Large eddy simulations of two basic configurations (decay of isotropic turbulence, and the academic plane channel flow) with heat transfer have been performed comparing several convection numerical schemes, in order to discuss their ability to evaluate temperature fluctuations properly. Results are compared with the available incompressible heat transfer direct numerical simulation data. It is shown that the use of regularizing schemes (such as high order upwind type schemes) for the temperature transport equation in combination with centered schemes for momentum transport equation gives better results than the use of centred schemes for both equations. Copyright © 2004 John Wiley & Sons, Ltd.

KEY WORDS: large eddy simulation; turbulent heat transfer; scalar transport; temperature; convection schemes; QUICK; FRAM limiter

1. INTRODUCTION

One of the major concerns of the thermo-hydraulic department (DTP) at the French Atomic Agency (CEA) is to study thermo-hydraulic phenomena that take place in nuclear plants, at nominal conditions as well as in possible critical conditions, in a huge part for safety studies.

The fluid flows of interest are essentially turbulent flows with high heat transfers. Among many, one of the possible tools to handle these problems relies on the development of specific methods for the simulation of unsteady turbulent flows such as the large eddy simulation (LES).

Comprehension and good forecast of what will be the characteristics of the heat transfers and temperature fluctuations is a major problem, specially if we focus on problems such as thermal fatigue. In fact, not only computations must provide good results for the mean temperature fields, but they also have to give accurate results (in frequency and amplitude) for the fluctuating temperatures: an under-estimation of the temperature fluctuations at the

*Correspondence to: A. Châtelain, CEA Grenoble, 17 Rue des Martyrs, 38054 Grenoble Cedex 9, France.
†E-mail: alexandre.chatelain@cea.fr
‡E-mail: frederic.ducros@cea.fr

Received 24 February 2003
Revised 22 July 2003

wall could lead to a rapid destruction of the wall material by thermal fatigue, thus generating bursts (leaks) and security problems.

A lot of work has been devoted to select 'good numerical methods for LES'. Although some work rely on the use of slightly diffusive methods, such as the ones involved in the so-called MILES (monotonically integrated LES) concept [1, 2], the general shared recommendations within the academic LES community are the following:

(i) use of non-diffusive schemes such as spectral methods or high order centred schemes for convection (see References [3–6]).
(ii) even if a particular phenomenon (such as contact discontinuity or shock occurrences) appears and requires specific numerical treatments (hybrid upwind and central schemes, see Reference [6]), the areas dominated by turbulence should basically be treated through centred schemes, or at least with 'as low numerical diffusion as possible'.

This choice clearly comes from good conservation properties associated to the centred schemes (kinetic energy for the momentum equation, temperature variance for the transport equation): conservation at a discrete level being ensured for some particular (skew-symmetric) formulations [3]. In addition when focusing on the momentum transport equations, Garnier *et al.* [5], showed that the use of regularizing schemes can completely hide the effect of the sub-grid-scale model. However centred convection schemes used to discretize the temperature equation in LES are known to generate possible numerical instabilities. No discussion is made about the sub-grid scale turbulence modelling (that could keep the temperature field between physical bounds) in the frame of this work since it is not the purpose of a SGS model to have this property but yes to represent the sub-grid scale effect on the resolved scales. Therefore a solution must be found on a numerical point of view.

These instabilities are responsible for non-physical over-estimated fluctuations of temperature for example, which is not in accordance with precise thermal fatigue predictions.

On the contrary, the use of stabilizing convection schemes tends to damp temperature fluctuations, which is not compatible with security prediction and against the idea of 'maximizing the constraints'.

Previous works involving direct numerical simulations rely on the use of a combination of centred scheme for the advection term in the momentum equation and regularizing (say Quick) scheme for the advection of temperature (see References [7, 8]). It is therefore tempting to use the same combination for LES (see also Reference [9]).

Considering the basic test case of forced convection in a channel flow configuration, the purposes of this paper consist of two points:

(i) illustrate the fact that the centred–centred combination for both momentum and temperature equations does not always give accurate results (it can lead to over-prediction of temperature fluctuations). This point is comforted by the work of Montreuil *et al.* [10] from which it seems possible to extrapolate that discrepancies between results and referenced solutions may be due to the numerical schemes and not to the SGS modelling. Also, a brief investigation shows that quality of the results are not improved when using an implicit time integration. This gives an idea for the behaviour of wall bounded flows. We will show that it is even worse for other types of flows, such as free shear flows (Tee junction).

(ii) investigate the behaviour of the combination 'centred scheme for momentum-regularizing scheme for temperature' and show some of its advantages and limits for LES of wall bounded flows.

This work makes part of a preliminary reflection before dealing with more complex geometries such as a 3D jet in a cross-flow at different temperatures with fluid–solid interaction. This preliminary work relies on the treatment of wall resolved flows (i.e. no wall functions are used).

2. LITERATURE SURVEY

Majority of available numerical results concerning fundamental and theoretical studies of unsteady heat transfer are done either by direct numerical simulation (DNS) or LES. DNS of such configurations are most of the time realized using kinetic energy conservative schemes [11–16].

Other authors [7, 8] have noticed some spurious behaviour of centred schemes for scalar transport and recommend the use of regularizing schemes for temperature transport for DNS, justifying their choice by former DNS based on high order (fifth order) upwind biased schemes [4]. But only few results are given for LES focusing on the heat transfer in the simple case of iso-thermal walls (see References [10, 17]).

In the case of Reference [10], LES computations were carried out for iso-flux boundary conditions and using a semi-implicit time integration technique. Advective terms are discretized using a second order centred scheme. The author made a parametric study with numerous sub-grid scale models for the SGS heat flux (Fickian as well as non-Fickian models) and observed an over-prediction of the resolved temperature fluctuations T_{rms} regardless of the SGS model, but obtained good mean profiles. The over-prediction of the peak value of the temperature fluctuations is between 30 and 40% for the simulations equivalent to our space discretization. Wang *et al.* [17] used a fully implicit time integration, as well as a third-order upwind scheme for advective terms but available literature results are limited to mean profiles for temperature.

Some authors have been investigating heated channel flows under buoyancy effects [18, 19]. Peng and Davidson [19] have studied a vertical channel flow with buoyancy effects using a second-order centred convection scheme and an implicit time integration. They found a good agreement between there T_{rms} fields and the available DNS data. Lee and Pletcher [18] made LES computations of a horizontal channel flow submitted to an unstably stratified temperature field, using the same numerical procedure as Reference [17].

These previous works dealing with passive scalar transport have not focused on the effect of the convection scheme in the case of LES, at least concerning the ability of predicting scalar fluctuations for wall bounded flows.

3. MODELLING FRAMEWORK

In the frame of the incompressible Navier–Stokes equation, temperature is considered in the present study as a passive scalar.

The modelling technique used here to compute these turbulent flows is the large eddy simulation. The continuous equations and continuous calculated fields are discretized in order to solve the governing equations. The discretizing process leads to a scale separation between the large (resolved) scales and the small (unresolved) scales of the fluid flow. It can thus be interpreted as a filtering operation. Following Reference [20], this can be seen as the combination of a spatial filter to the governing equations in order to retrieve and calculate explicitly the large scales of the fluid motion in our computation, while the action of the small scales (smaller than the filter width, usually the grid size) is modelled by a SGS model. This basic underlying justification is that large scales of the motion are the ones which are responsible for most of the dynamics of the fluid flow and are long-living, whilst small scales of turbulence are more generic, and account for the largest part of the turbulent energy dissipation (see the standard literature on the topic such as Reference [21]).

3.1. Governing equations and physical modelling

As the present work mainly relies on numerical aspects, the governing equations and the physical modelling are only briefly described: they indeed rely on standard approaches [22, 23].

3.1.1. Governing equations and related physical constraints. For an incompressible flow, the filtered Navier–Stokes equation, as well as the temperature equation, read as follows (if we admit that the filter has the permutation property with both time and spatial derivatives), where the $\widetilde{(\,)}$ stands for a standard filtering operator:

$$\frac{\partial \widetilde{u_i}}{\partial t} + \frac{\partial \widetilde{u_j}\widetilde{u_i}}{\partial x_j} = -\frac{1}{\rho}\frac{\partial \tilde{p}}{\partial x_i} + \frac{\partial}{\partial x_j}(2\nu\widetilde{S_{ij}} + \tau_{ij}) \tag{1}$$

and

$$\frac{\partial \tilde{T}}{\partial t} + \frac{\partial \widetilde{u_i}\tilde{T}}{\partial x_i} = \frac{\partial}{\partial x_i}\left(\kappa\frac{\partial \tilde{T}}{\partial x_i} + \Theta_i\right) \tag{2}$$

Here τ_{ij} is the sub-grid-scale (SGS) stress tensor and Θ_i is the SGS turbulent heat flux. These SGS terms account for the energy transfer from the large scales to the small scales of turbulence [21]. Most part of the actual models are based on a Boussinesq hypothesis, which relates the SGS tensor to the strain-rate tensor by means of a turbulent eddy viscosity, following relation (3):

$$\tau_{ij} = \widetilde{u_i}\widetilde{u_j} - \widetilde{u_i u_j} = 2\nu_t\tilde{S}_{ij} + \frac{1}{3}\delta_{ij}\tau_{kk}; \quad \tilde{S}_{ij} = \frac{1}{2}\left(\frac{\partial \tilde{u}_i}{\partial x_j} + \frac{\partial \tilde{u}_j}{\partial x_i}\right) \tag{3}$$

As for the SGS heat flux, Θ_i, a Fickian approach of the problem is commonly assumed, thus relating the SGS heat flux to the resolved temperature gradient by means of a turbulent diffusivity as seen in equation (4):

$$\Theta_i = \widetilde{u_i}\tilde{T} - \widetilde{u_i T} = \kappa_t\frac{\partial \tilde{T}}{\partial x_i} \tag{4}$$

A point that can raise an issue is the implicit assumption that the LES filter keeps the same numerical bounds for the filtered equation than for the non-filtered equation. This could become the subject of a whole research topic but is not the purpose of this work.

Indeed, given a set of initial and boundary conditions, let us consider that the physical transport of a quantity ϕ respects the following physics:

$$\forall t, \forall \mathbf{x} : \xi_1 \leqslant \phi(\mathbf{x}, t) \leqslant \xi_2$$

What enables one to write that the filtered equation:

$$\frac{\partial \tilde{\phi}}{\partial t} + \frac{\partial \widetilde{u_i}\tilde{\phi}}{\partial x_i} = \frac{\partial}{\partial x_i}\left((\alpha + \alpha_t)\frac{\partial \tilde{\phi}}{\partial x_i}\right)$$

(from which all the terms resulting from any non-commutation between the filter operator $\widetilde{(\,)}$ and the spatial derivatives have been omitted) respects the following statement (i.e. it follows the same physical evolution):

$$\forall t, \forall \mathbf{x} : \xi_1 \leqslant \tilde{\phi}(\mathbf{x}, t) \leqslant \xi_2$$

is that the resulting filter should be regularizing and monotonic.

By resulting filter, one has to read it as the sum of the combined effects on the solution of the mesh discretization (cut-off at $2\tilde{\Delta}$, $\tilde{\Delta}$ being a measure of the grid spacing), of the eddy viscosity and of the numerical schemes involved in the equation resolution.

Therefore, two approaches can be seen to strengthen the above statement. In the first one, it can be assumed that the diffusive effects, the realizability of the sub-grid scale model in conjunction with a well chosen filter operator, will keep the filtered quantity evolution bounded by the physical boundaries. In the second one, the respect of the physical boundary evolution is imposed for the filtered quantity evolution, which should be respected given a proper set of numerical schemes. The latter will be retained for the present paper.

3.1.2. SGS stress modelling. The candidate retained for our eddy viscosity model is the WALE (wall-adapting local eddy-viscosity) model from Nicoud and Ducros [24].

The main idea of this model is to recover the proper behaviour of the eddy viscosity near the wall ($o(y^3)$) in case of wall-bounded flows, while preserving interesting properties such as the capacity to provide no eddy-viscosity in case of vanishing turbulence (property required for the transition from laminar to turbulent states). Major interest of this model first rely on the fact that it needs no information on the direction and distance from the wall (avoiding the use of any damping function) thus being really suitable in unstructured grids where evaluating a distance to the wall is precarious.

3.1.3. SGS heat flux modelling. The SGS heat flux term is modelled using the assumption of a SGS Prandtl number, Pr_t, which is the simplest and usual way to model this term:

$$\kappa_t = \frac{\nu_t}{Pr_t} \tag{5}$$

One must keep in mind that the turbulent Prandtl number is commonly associated to a statistical approach of turbulence (ensemble or time averaging), whereas the SGS Prandtl number refers to a filtered approach of the turbulent field and depends of both time and space, as a combination of Equations (3)–(5).

Therefore, there is no obvious reason why these two definitions would lead to the same values since they do not define the same variable.

However, the assumption that the two (different) filtering formulations give approximately the same value for the turbulent and sub-grid scale Prandtl number relies on previous LES works and related literature [10, 17].

Montreuil *et al*. [10] show for example that the evolution of the sub-grid scale Prandtl number across the channel is not constant but remains between 0.6 (in the middle of the channel) and 1.2 (maximum value at about $y^+ \simeq 20$). Moreover, Wang *et al.* in their LES work [17] of turbulent plane channel flow, show the evolution of the modelled sub-grid scale turbulent Prandtl number which varies between 1 (at the wall) and 0.5 (in the middle of the channel).

Here Pr_t is assumed constant and equal to 0.9. This value is motivated by the DNS work of authors like Lyons *et al.* [12], Nicoud [16] and Kim *et al.* [11] who found an evolution of Pr_t approximately constant and equal to 0.9. The work of Kasagi *et al.* reported in Reference [14] indicates a value of Pr_t almost equal to 1. These SGS models were used for all computations of this paper to derive only the influence of the advection scheme. More sophisticated models can be used (see References [10, 17]), but this point is not the key issue of the present study.

3.2. Numerical methods

All computations discussed in this paper were done using the TRIO_U/PRICELES code developed at CEA Grenoble [25]. This code is mainly intended to deal with LES in thermo-hydraulics, using structured or unstructured grids under the incompressible or low-Mach number approximations.

In this paper, calculations were done using structured grids. Unknowns (pressure, velocity and temperature) are located on a staggered grid [35].

The discrete form of the incompressible Navier–Stokes equation is solved in matrix form by a projection method. The Poisson equation for the pressure is solved by a conjugate gradient method with a SSOR preconditionning to ensure a zero divergence field (usual convergence limit is 10^{-8}). Once it is determined, it is replaced in the momentum equation, so that velocity is calculated and can be used in the temperature equation. A second order centred advection scheme was used for the momentum equation.

Different convection schemes were compared for the temperature advection term (in its conservative form) in the heat equation: Centred fourth order (denoted by $C4$), Upwind first order ($U1$) and Quick third order with FRAM limiter ($Q3$) (See Appendix A for details). Results concerning the use of the second order Centred scheme for temperature transport are not presented in this work, but has been shown to give the same behaviour and results as the $C4$ scheme: the effects interested herein are due to the centred nature of the schemes and not to their order.

Time advancement is done using a third order Runge–Kutta explicit time integration scheme (denoted by RK3) (see Reference [26]) except for one simulation where we have made use of a Cranck–Nicolson scheme (denoted by CN).

4. RESULTS

The present reflection will rely on simulations performed on three configurations:

(i) a 2D Tee junction that illustrates the problem of handling contact discontinuity within a turbulent-like context. As already recalled in some study [8], this will show that centred type schemes lead to spurious oscillations of the temperature field, whereas regularizing schemes show acceptable physical results;
(ii) a freely decaying isotropic turbulence that will test the different schemes against their capabilities of handling fully turbulent flows;
(iii) the periodic channel flow to cope with the wall bounded flow type problems.

4.1. 2D TEE junction

Following previous study reported in Reference [9], centred scheme may lead to numerical instability for scalar equation with inflow/outflow conditions. This is illustrated here by the present configuration that concerns a simple two dimensional unsteady flow with different temperatures developing in a Tee junction (see Figure 1). The objective is not to reach physical results as turbulent mixing is concerned since the configuration is 2D. Attention was only payed to the temperature field (especially on its bounds), bearing in mind that the simulation results at the early stages of the phenomenon do not rely only on SGS modelling but also on the numerical treatment of the contact discontinuity.

In particular, the large structures observed downstream are due to the 2D simulation and should disappear when turning to 3D.

The initial condition is a uniform temperature field at $T_2 = 550\,\mathrm{K}$ and downward parabolic velocity field in the upper part and a uniform temperature of $T_1 = 500\,\mathrm{K}$ and a parabolic velocity field in the lower part of the domain. Reynolds number is equal to 1546.

Boundary conditions are adiabatic and no-slip condition on the walls. Outlet boundary condition is an imposed uniform 0 pressure. The inlet boundary conditions are (for simplicity) two parabolic velocity profiles of same maximum velocity and different uniform temperatures (500 and 550 K). Two meshes of 313×40 (for the lower flow) and 40×80 (for the upper

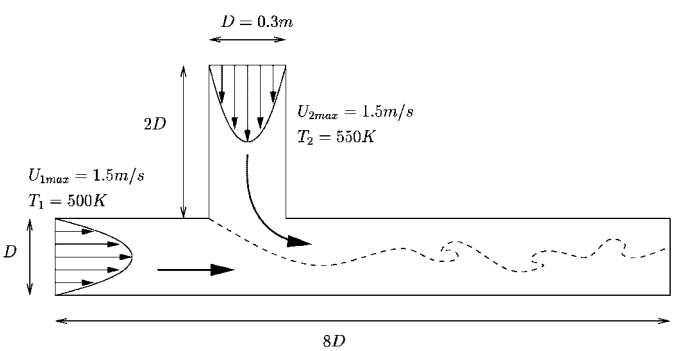

Figure 1. Configuration of the unsteady 2D Tee junction. The dashed line stands for a possible representation of the instantaneous location of temperature gradients.

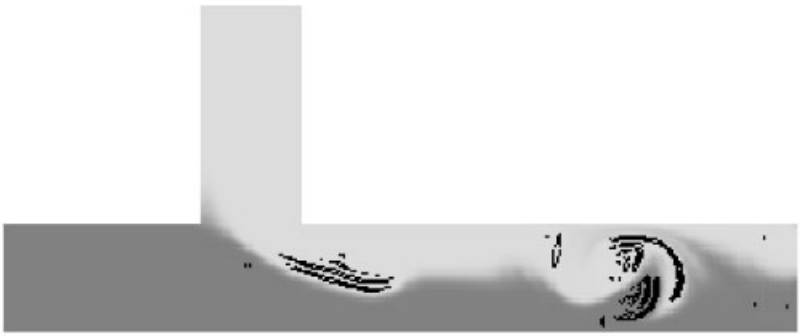

Figure 2. Instantaneous temperature fields in a 2D unsteady Tee junction at $t = 12.2$ s (8 recirculation times)—non-physical temperature regions (i.e. out of limits) are denoted by dark contours. Centred 4th order; $T_{max} = 554.9$ K $- T_{min} = 494$ K.

Figure 3. Instantaneous temperature fields in a 2D unsteady Tee junction at $t = 12.2$ s (8 recirculation times)—non-physical temperature regions (i.e. out of limits) are denoted by dark contours. Quick; $T_{max} = 550$ K $- T_{min} = 500$ K.

incoming flow) elements constitute the complete grid domain. No sub-grid scale model was used in this section.

First requirement of such a simulation is that temperature field should stay bounded by physical imposed temperatures. The critical zones (i.e. the zone where most of the points reach temperatures beyond physical limits, see Figure 2) are of course located where mixing is the highest. Moreover, the diffusive behaviour of the different convection schemes is clearly seen in this situation. Indeed, the $U1$ scheme shows a temperature field and a contact line between the hot and cold fluid which is much more blurred than the $Q3$ or $C4$ scheme (Figures 3 and 4).

Figure 5 shows the time evolution of the highest temperature observed in the domain at each time step. As seen in this figure, we see the important stabilizing effect of the temperature convection scheme: using the $Q3$ or the $U1$ scheme keeps the temperature field within physical boundaries, whereas the $C4$ scheme creates oscillations beyond the two inlet temperatures.

Figure 4. Instantaneous temperature fields in a 2D unsteady Tee junction at $t = 12.2$ s (8 recirculation times)—non-physical temperature regions (i.e. out of limits) are denoted by dark contours. Upwind; $T_{max} = 550\,\mathrm{K} - T_{min} = 500\,\mathrm{K}$.

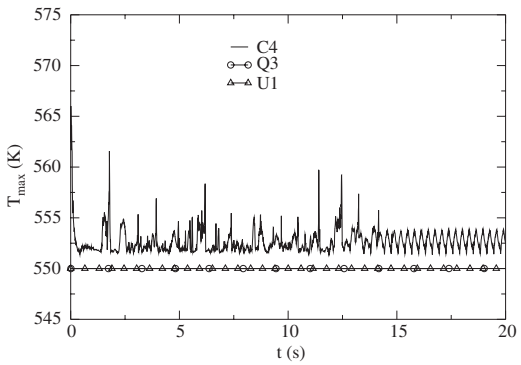

Figure 5. 2D Tee junction: temporal record of maximum temperature in the physical domain.

4.2. Freely decaying isotropic turbulence with passive scalar transport

The case of isotropic turbulence decay with passive scalar transport is of particular interest to test the numerical diffusion of numerical convection schemes since there are a lot of available results throughout the literature concerning, for example, enstrophy or energy decay [23].

Expected temperature behaviour in these simulations is to stay bounded by the initial temperature extrema, while the fluid temperature is homogenized by both the fluid motion and the molecular diffusion and tends to a steady state where the fluid is at the mean homogeneous temperature.

These simulations were performed in the case of infinite Reynolds number in which the dissipation is to be attributed to the action of the SGS modelling (see Table I).

The domain is a cube of dimensions $(2\pi)^3$, periodic in every direction and discretized with $(32)^3$ elements on a regular mesh.

The initial condition, for both temperature and velocity, is a three-dimensional random isotropic field whose kinetic energy peaks at a wavenumber of $k_i(0) = 4$. The temperature field is chosen so that the mean homogeneous temperature is $\langle T \rangle = 100\,\mathrm{K}$ ($\langle\ \rangle$ operator stands

Table I. Parameters for the freely decaying isotropic turbulence with passive scalar transport.

Case	Mesh grid	$U \bigtriangledown U$	$U \bigtriangledown T$	Time int.
1	$(32)^3$	$C2$	$C4$	RK3
2	$(32)^3$	$C2$	$Q3$	RK3
3	$(32)^3$	$C2$	$U1$	RK3

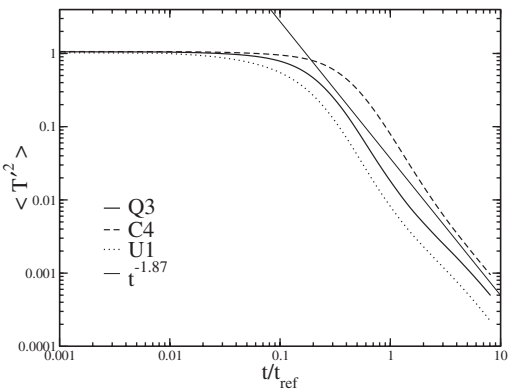

Figure 6. Time evolution of temperature variance. The -1.87 slope reference is taken in Reference [27].

for the classical spatial average) and to have an initial mean temperature variance equal to 1 ($T(\mathbf{x}, t=0) = \langle T \rangle((\kappa - \langle \kappa \rangle)/100. + 1.)$; where κ is the local kinetic energy). As a consequence, the temperature field is as smooth as the velocity field at $t=0$. The initial maximum (resp. minimum) to mean temperature ratio in the domain is $T_{0\,\max}/\langle T \rangle = 1.0443$ (resp. $T_{0\,\min}/\langle T \rangle = 0.9577$).

A characteristic time scale, which is the large-eddy turnover time, is defined as: $t_{\text{ref}} = L/\sqrt{E_c(0)}$ where L is a characteristic length of the eddies containing most of the initial energy.

Three simulations were done using different convection schemes, but on same grid and with same time integration (RK3) and momentum convection scheme (C2).

The Figure 6 represents the time evolution of temperature variance, and Figure 7 shows the decay of temperature enstrophy $D_T(t) = \frac{1}{2}\langle(\boldsymbol{\nabla} T)^2\rangle$ (see Reference [23] for an extensive reference).

The decay law in $t^{-1.87}$ of the temperature variance, shown for example in the work of Métais and Lesieur [27], is recovered reasonably well.

The dissipative effects of the upwind type schemes ($U1$, $Q3$) in the evolution of the temperature enstrophy can be easily seen, since these schemes do not reproduce the initial increase and its maximum value as can also be observed in the velocity enstrophy D with energy conservative schemes.

Considering only results on the temperature variance and on the enstrophy, the best results are achieved with the $C4$ scheme compared to the other upwind type schemes, since the $Q3$ scheme tends to damp the enstrophy and variance evolution of temperature during the simulation.

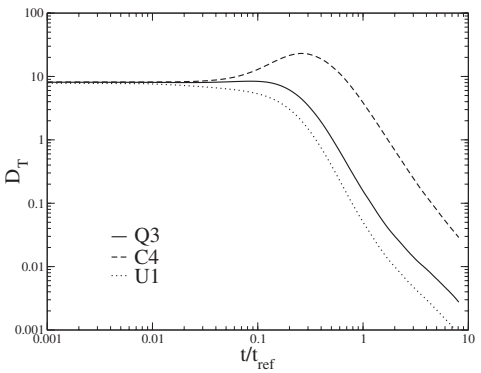

Figure 7. Time evolution of temperature enstrophy.

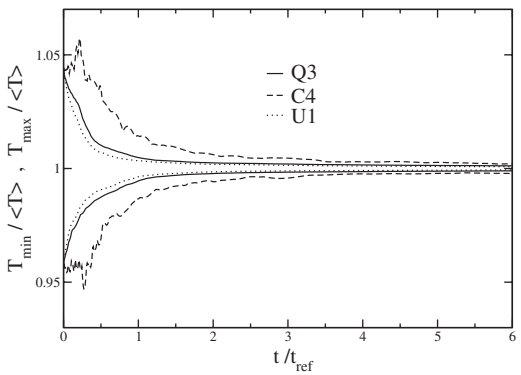

Figure 8. Time evolution of the extrema of the values of temperature in the decaying isotropic turbulence.

The evolution of the extrema values of the temperature field is given in Figure 8 and illustrates the fact that initial values are not 'physically bounded' for the $C4$ scheme simulation. However, $U1$ and $Q3$ schemes homogenize the temperature field faster than the $C4$ scheme.

The Figure 9 confirms this tendency. Classical influence of the stabilizing schemes compared to the kinetic energy conservative scheme can be observed in the representation of the temperature field PDF (Figure 9) where the first schemes tend to gaussianize the PDF. This effect is known to take place in the small scales [27]. In Figure 9, vertical continuous lines represent the initial maximum and minimum temperatures. These boundaries should fix physical bounds for the temperature field since the scalar will tend to homogenize and should not create temperature values beyond these bounds. However, it is seen that for the $C4$ conservative scheme, temperature values are out of the initial physical bounds due to the numerical instabilities created during the first moments of turbulence decay.

The damping effect of the different convection schemes is illustrated in Figures 10–12 which show the temperature field at the same time $t/t_{\text{ref}} = 0.75$. These three pictures of the flow show that the temperature field exhibits less and less small structures as the scheme is more and

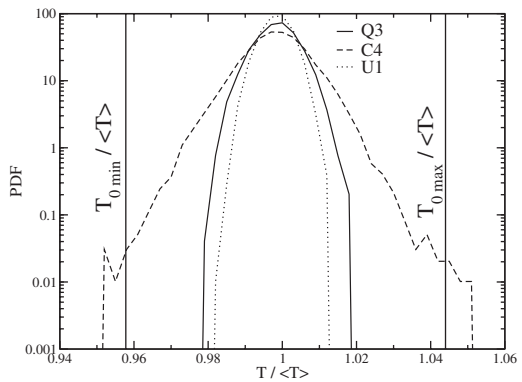

Figure 9. PDF of the scalar field in an isotropic turbulence at $t/t_{\text{ref}} = 0.27$. The vertical lines stand for the physical (initial maximum and minimum values) bounds.

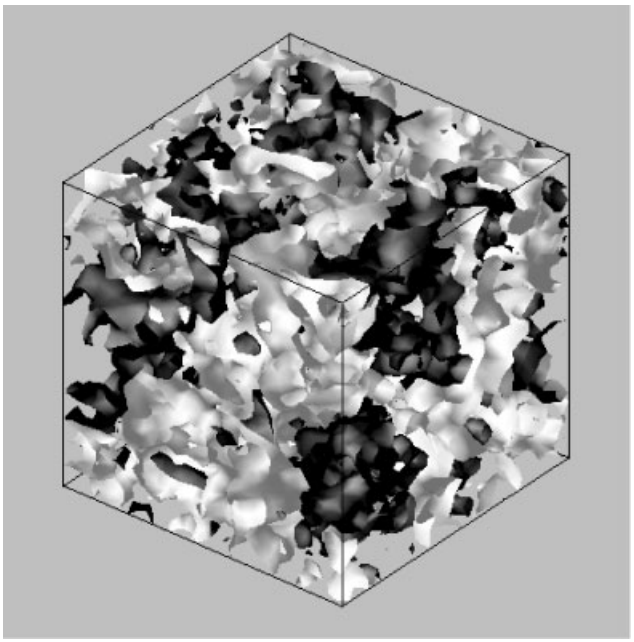

Figure 10. Isotropic turbulence—visualization of the damping effect of the advection scheme: isosurfaces of temperature are shown at same time $t/t_{\text{ref}} = 0.75$—Black: $T/\langle T\rangle = 1.002$—White: $T/\langle T\rangle = 0.998$. ($T_{\max}$ and $T_{\min}$ values can be taken from Figure 8) Fourth order centred.

more diffusive. However, it should be noticed that the use of the Q3 scheme is compatible with the occurrence of small turbulent structures (typically resolved within 5 grid points which is reasonable in the LES framework). These damping effects were also observed in the work of Garnier *et al.* (see Reference [5]).

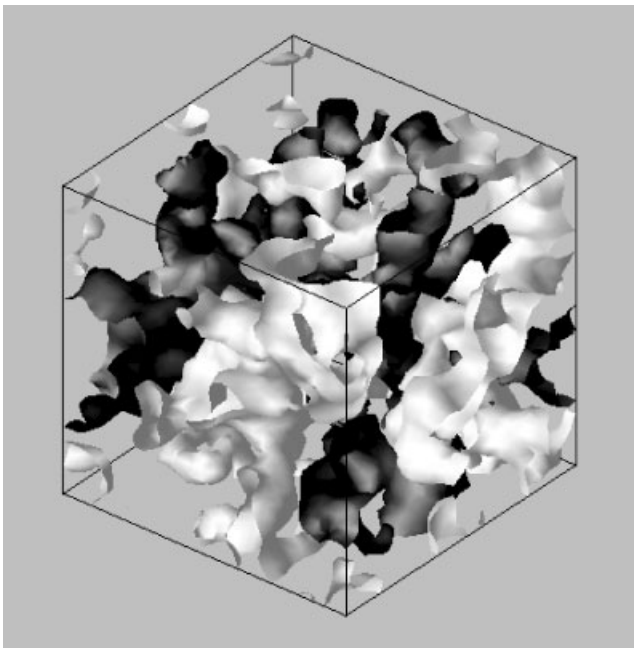

Figure 11. Isotropic turbulence—visualization of the damping effect of the advection scheme: isosurfaces of temperature are shown at same time $t/t_{\text{ref}} = 0.75$—Black: $T/\langle T \rangle = 1.002$—White: $T/\langle T \rangle = 0.998$. ($T_{\max}$ and $T_{\min}$ values can be taken from Figure 8) Third order quick FRAM.

Considering all criteria (time evolution of variance, enstrophy and of the extrema of temperature), a compromise is to be found between a numerical method (centred) which reproduces correctly intermittency phenomena but may exhibit non-physical behaviours, and other methods (regularizing) which respects physical boundaries but may show limited qualities to reproduce all type of turbulent events such as intermittency phenomena.

Given this reflection, we shall now investigate these two methods for the channel flow configuration.

4.3. Plane channel flow

4.3.1. Explicit time integration simulations. Most of our interest was focused on the plane channel configuration with different imposed iso-thermal wall temperatures since it is a well documented test case, as already seen in the literature survey.

The computational domain is the academic periodic channel flow. Boundary conditions in the x (streamwise), y (wall normal) and z (spanwise) directions are respectively periodic, no-slip, and periodic boundary conditions (Figure 13). Both walls are set at different but constant temperatures T_1 and $T_2 > T_1$ (with a ratio of 1.01 but, since the incompressible Navier–Stokes equations are solved, with uniform and constant density and since there is no buoyancy force, the temperature ratio is irrelevant in this study and any value could have been used).

Domain dimensions in wall units are $L_{x^+} = 2262, L_{y^+} = 360, L_{z^+} = 565$. The number of grid points is $64 \times 55 \times 40$, thus resulting in a well resolved LES for the LES Mesh 1 case. In

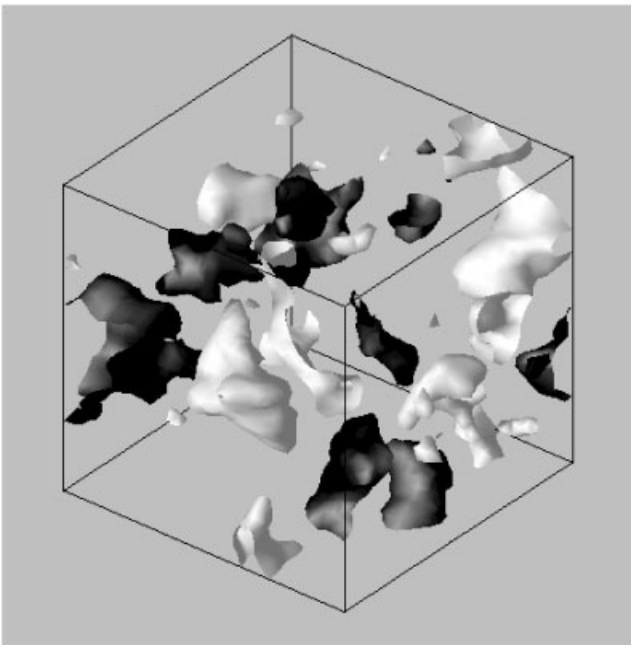

Figure 12. Isotropic turbulence—visualization of the damping effect of the advection scheme: isosurfaces of temperature are shown at same time $t/t_{\mathrm{ref}} = 0.75$—Black: $T/\langle T\rangle = 1.002$—White: $T/\langle T\rangle = 0.998$. ($T_{\max}$ and $T_{\min}$ values can be taken from Figure 8) First order upwind.

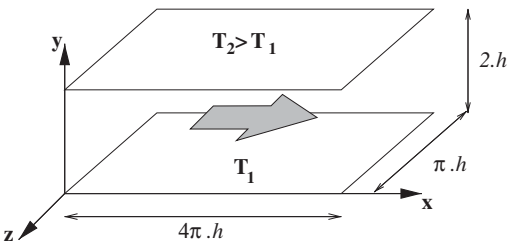

Figure 13. Thermal channel flow configuration.

the LES Mesh 2 case, the number of grid points is $64 \times 55 \times 65$. Grid spacings and mesh characteristics are given in Table II. The Prandtl number of the fluid is 0.71. The bulk Reynolds number $Re_{\mathrm{b}} = U_{\mathrm{b}}h/\nu$ is 2762. Dean's correlation [28] would predict, in the present case, a turbulent Reynolds number of 180. h is the channel half-height and U_{b} is the bulk velocity given by $U_{\mathrm{b}} = \frac{1}{2h}\int_0^{2h} U \,\mathrm{d}y$.

Since temperature is a passive scalar, the velocity field is the same for every simulation done at the same Re_τ, whatever the scalar field may look like. Velocity field is initialized with a parabolic Poiseuille flow with a white noise perturbation on all three components, and initial temperature field corresponds to a linear laminar profile.

Table II. DNS parameters for the channel flow configuration given by other authors together with present LES mesh parameters.

	Δx^+	Δy_w^+	Δy_c^+	Δz^+	Re_b	Re_τ	Nu
Kasagi *et al.* [31]	18.4	0.08	4.9	7.36	2290	150	13.4
Kim *et al.* [30]	12	0.05	4.4	7	2800	180	—
Debusschere *et al.* [32]	9.7	1.9	1.9	5.9	3000	186	24.3
Nicoud [15]	20	0.3	9	6	2855	180	NA
LES Mesh 1	36	1	11	14.5			
LES Mesh 2	36	1	11	8.8			

Δy_w^+ stands for the first grid point at the wall; Δy_c^+ stands for the centreline grid-spacing. NA means data is not available for this simulation.

Table III. LES parameters and global results for the channel flow configuration (mesh parameters are given in Table II).

Case	Mesh	$U \bigtriangledown T$	Model	Time integration	$Re_\tau/Re_{\tau\ \text{target}}$	Nu
$C4-F$	2	$C4$	yes	$RK3$	180/180	23.3
$C4$	1	$C4$	yes	$RK3$	177/180	21.7
$Q3$	1	$Q3$	yes	$RK3$	177/180	22.2
$U1$	1	$U1$	yes	$RK3$	177/180	20.9
$C4-Imp$	1	$C4$	yes	CN	176/180	22
$C4-noMod$	1	$C4$	no	$RK3$	177/180	21.7
$Q3-noMod$	1	$Q3$	no	$RK3$	177/180	22.1

Imp refers to the implicit time integration method of Cranck–Nicolson (denoted by CN). F stands for refined mesh. *noMod* means that no SGS model was used for the temperature equation.

The forcing term in the momentum equation used to keep a constant flow rate is the one proposed by Rollet–Miet [29] and reads as

$$f_v(t_{n+1}) = f_v(t_n) + \frac{2(Q_0 - Q(t_n)) - (Q_0 - Q(t_{n-1}))}{\Delta t S} \tag{6}$$

where $f_v(t_n)$ is the forcing term at time step n, Q_0 is the initial flow rate, $Q(t_n)$ is the flow rate at time step n, Δt is the time step and S is the section of the plane channel in the main flow direction.

No source term is used in the scalar equation since two different temperatures are imposed on both walls.

All comparison parameters between simulations are given in Table III.

Mean profiles and rms fluctuations will be given in dimensionless form using the following definitions of the friction velocity and temperature:

$$u_\tau^2 = \nu \left(\frac{\partial u}{\partial y}\right)_w \quad \text{and} \quad T_\tau = \frac{\lambda(\partial T/\partial y)_w}{\rho C_p u_\tau}$$

First and second order moment quantities are averaged in the x and z homogeneous directions, and in time for a period of 45–50 transit times to ensure statistically converged profiles.

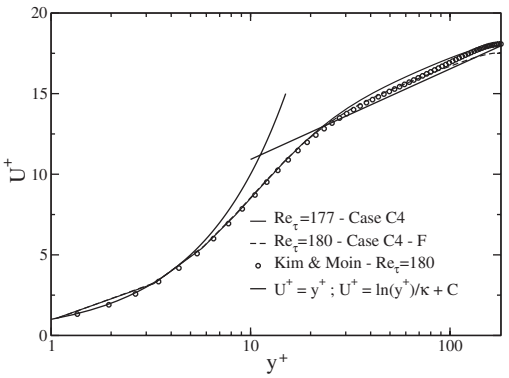

Figure 14. Distribution of mean streamwise resolved velocity in wall co-ordinates.

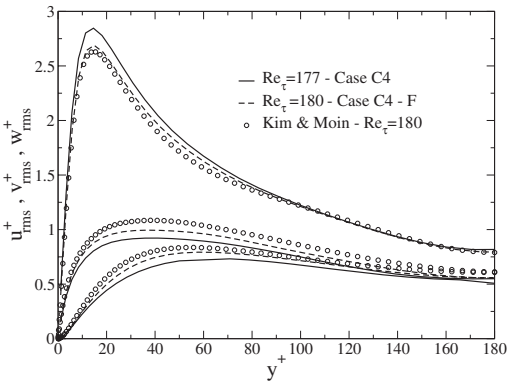

Figure 15. Distribution of resolved velocity fluctuations in wall co-ordinates.

A transit time is defined as the physical time for the fluid at the bulk velocity to make a complete pass through the channel length.

Results for the velocity field are given in Figures 14 and 15 and are compared to the DNS data from Kim and Moin [30] whose incompressible calculations are done for a bulk Reynolds number of 2800 and a target turbulent Reynolds number of 180.

Good agreement is reached for our LES results: the usual behaviour is observed, that is to say a small over-prediction (8%) of the streamwise velocity fluctuations u^+_{rms} and a slight under-estimation of the two other components: v^+_{rms} and w^+_{rms}. Peak locations are also well predicted.

Mean velocity profile is found to be in good agreement with DNS data and classical linear and logarithmic behaviour. Calculation with a refined grid (Case $C4 - F$) has been done to check the consistency of the results. The expected behaviour is that by refining in the spanwise direction, fluctuations in the z direction will be more precisely appreciated and a better distribution in the fluctuating field will be reached, hence diminishing the fluctuations

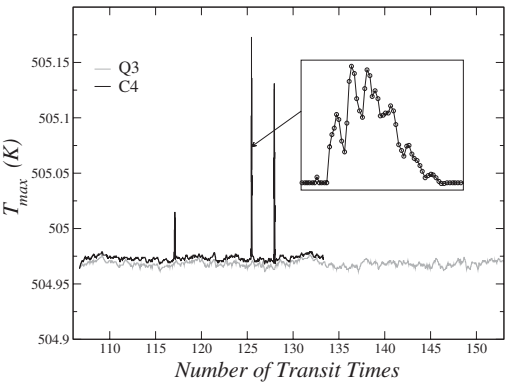

Figure 16. Time evolution of computational domain maximum temperature in a turbulent channel flow (upper physical bound is 505 K).

in the streamwise direction and increasing the v^+_{rms} component. Such reflection is found to be in agreement with the obtained results.

Figure 16 shows the evolution in time of the maximum value of the temperature in the computational domain (minimum value would show a similar behaviour). Non-physical temperatures are also observed in this configuration with the $C4$ scheme (Case $C4-F$) but with smaller frequency. On the other hand, we see that the $Q3$ scheme (Case $Q3$) has a better behaviour and that maximum fluctuations have a smaller level than the $C4$ scheme.

However the amplitude of variation of the maximum of temperature is of same order for the $C4$ and $Q3$ simulations when physical bounds are respected (for example between the 110 and 115 transit times in Figure 16).

This test is less severe than the previous ones (Sections 4.1 and 4.2) since there is little chance to have temperature contact discontinuities such as in a cross-flow jet. However, the same behaviour is observed for the extrema temperature as in the other configurations, but with less non-physical events.

Profiles for mean and fluctuating temperature are given in Figures 17 and 18. Results are compared to DNS data from Kasagi *et al.* [15] ($Re_\tau = 150$, $Pr = 0.71$), Debusschere *et al.* [33] ($Re_\tau = 186$, $Pr = 0.7$) and Nicoud [15] ($Re_\tau = 180$, $Pr = 0.76$) who made the same simulation with constant but different temperatures at the walls.

Mean dimensionless temperature profile given in Figure 17 is seen to recover the proper behaviour near the vicinity of the wall in $T^+ \rightarrow Pr_{y^+}$ and in the logarithmic zone.

No real difference was observed on the mean profile of temperature when changing convection scheme.

However, non negligible effects are seen on the temperature fluctuations (Figure 18): the $C4$ scheme overestimates the maximum fluctuations level (by 30%) in the same way as it was observed in the work done by Montreuil *et al.* [10]. The author showed that the overprediction of the peak maximum value reaches about 10–25%, depending on the type of SGS heat flux model used and on the resolution. The work of Montreuil *et al.* was compared to the DNS data of Kim and Moin [11] of a channel flow where temperature is produced uniformly in the flow and removed at the walls kept at constant and equal temperatures.

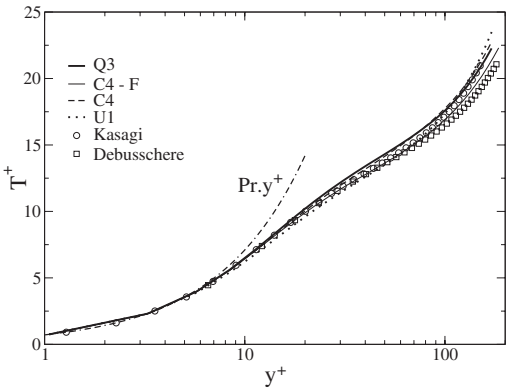

Figure 17. Distribution of mean resolved temperature in wall coordinates (For Debusschere and Kasagi data, only 1 point out of 3 and 1 point out of 2, respectively are represented).

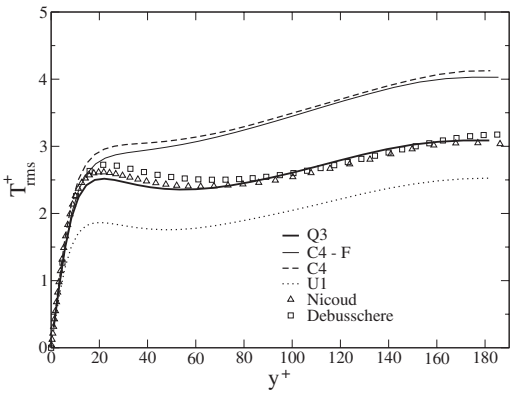

Figure 18. Distribution of resolved temperature fluctuations in wall co-ordinates.

Comparing results of the $C4$ scheme with the standard mesh (Case $C4$) and the ones obtained with the refined grid (Case $C4-F$) shows consistency with the chosen numerical method. As can be seen in Figures 17 and 18, results are only slightly improved when refining in the z direction. Moreover, the reduction of the rms fluctuations is negligible compared to the initial over-prediction.

The 'good' result obtained for T^+_{rms} with the $Q3$ scheme should also be analyzed looking at the basic $T_{\mathrm{rms}}/\Delta T$ quantity (see Figure 19).

The result provided by the $Q3$ scheme leads to a slight under-prediction of $T_{\mathrm{rms}}/\Delta T$, whereas $C4$ scheme leads to a clear over-prediction. However, it must be noticed that the near-wall behaviour reaches a better result with the $C4$ scheme than with the $Q3$ scheme, even if afterwards fluctuations are monotonous and do not show a proper temperature fluctuation profile.

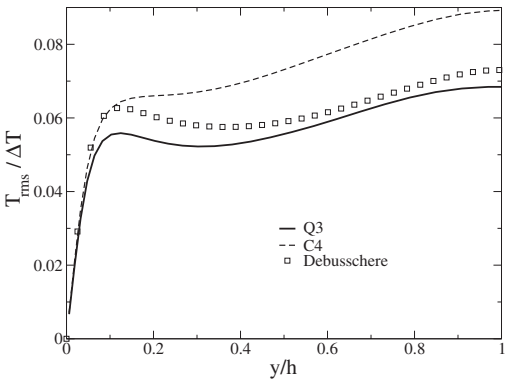

Figure 19. Distribution of temperature profiles undimensionalized by the temperature difference on the walls.

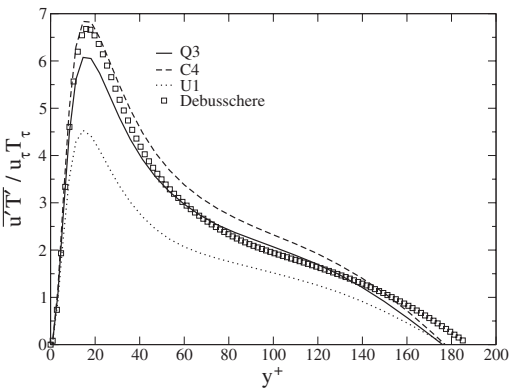

Figure 20. Resolved streamwise heat flux profile in the turbulent channel flow.

This can lead to a specific analysis and proposition for numerical scheme (see Section 5).

Comparing the results obtained for the Nusselt number (see Table III), defined as (see Reference [17]):

$$Nu = \frac{4h}{T_b - T_w} \frac{\partial T}{\partial y}_w$$

where T_b is the bulk temperature and T_w is the temperature at the wall, there is good agreement with the available correlation of Kays and Crawford [33] ($Nu = 0.04\, Re_b^{0.8} Pr^{0.3}$) at $Re_b = 2762$ and the DNS data of Debusschere *et al.* which correspond, respectively, to $Nu_{K\&C} \approx 20.4$ and $Nu = 24.3$.

All simulations lead to approximately the same value of Nu showing a small dependence of the convection scheme on the overall heat transfer.

Streamwise and normal heat flux profiles are given in Figures 20 and 21, respectively. Good agreement is achieved compared to the DNS results, and little difference is observed when

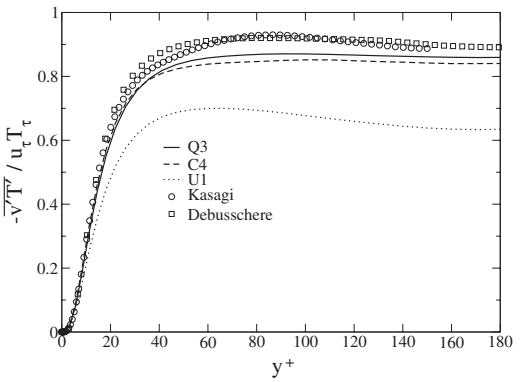

Figure 21. Resolved normal heat flux profile in the turbulent channel flow.

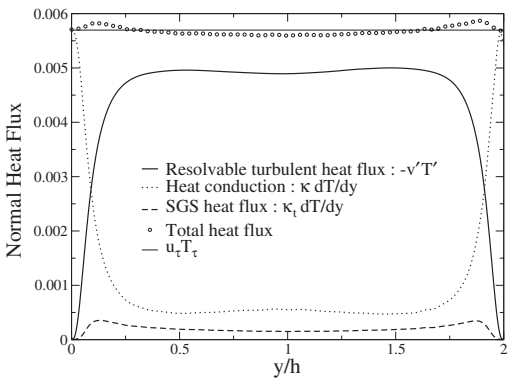

Figure 22. Normal heat flux budget for the $Q3$ scheme.

comparing results using the different convection schemes, except for the $U1$ scheme which shows damped results: an 8% under-prediction is obtained for the streamwise heat flux using the $Q3$ scheme.

Budget for the wall normal heat flux was calculated (and shown in Figure 22) to recover the budget equation which reads, in the case of isothermal walls configuration, as follows:

$$-\overline{v'T'} + (\kappa + \kappa_t)\frac{\partial \bar{T}}{\partial y} = u_\tau T_\tau \tag{7}$$

where the $\overline{(\,)}$ is here a time average operator.

The different terms of Equation (7) are, from left to right, the resolved turbulent heat flux, heat conduction, modelled SGS turbulent heat flux in the left hand side, and the total normal heat flux in the right hand side.

Figure 22 shows the budget in the case of the $Q3$ convection scheme, while results obtained for the $C4$ scheme are similar. The obtained profiles have the classic behaviour, where

the contribution of the sub-grid-scale model is relatively small since it is a quite well resolved LES.

4.3.2. Effect of implicit time integration. An attempt to derive the effect of an implicit time integration on the behaviour of the temperature field was done on the heated channel flow as well. The objective is to measure the ability of implicit schemes to limit spurious temperature values in case of use of centred scheme for convection.

Two major characteristics can be expected from the use of an implicit approach, which are: either large time steps are desired to accelerate convergence or time advancement; or extreme values wish to be smoothed in case of rapid dynamics.

The first point is not of interest in this framework since it is known that in wall-resolved LES use of too large CFL may lead to an underestimation of the turbulence intensities since it does an implicit filtering operation on the wall-region dynamics.

However, the second point is of interest since we want to measure an eventual smoothing behaviour on the temperature dynamics, even-though it is known that in the test case of a convected top hat signal, oscillations are created near the discontinuities which are not suppressed even in the implicit case in conjunction with a CFL number equal to 1.

The used time integration in this section is a classical implicit Cranck–Nicolson scheme, corresponding to the test Case $C4 - Imp$ (see Table III).

The implementation of the Cranck–Nicolson scheme reads as follows: starting from solution U^n at time step (n), an intermediate solution $U^{n+1/2}$ is estimated by means of an implicit method where all terms are implicit

$$U^{n+1/2} = U^n + \mathrm{Res}^{n+1/2}\frac{\Delta t}{2} \tag{8}$$

to calculate the value of the residual Res at the intermediate time step $(n + \frac{1}{2})$ that will be used in the explicit time step from (n) to $(n + 1)$:

$$\frac{U^{n+1} - U^n}{\Delta t} = \mathrm{Res}^{n+1/2} \tag{9}$$

In the implicit part for the estimation of the residual at $(n + 1/2)$, all terms all implicited and iterative procedure is applied until a certain threshold is reached.

The selected time stepping corresponds to a Courant–Friedrich–Lewy number around 0.8, as for the explicit simulation.

Results for the mean and fluctuating temperature profile are given in Figures 23 and 24, respectively.

We found slightly better results using the Cranck–Nicolson scheme in addition with the $C4$ scheme. Nevertheless, no significant improvement is achieved with this method: mean profile is in better agreement with given DNS data, still fluctuations are only reduced by 3% and represent an over-prediction of 26% referring to the DNS results. This over-prediction is compatible with the results of Montreuil *et al.* [10] who used a semi-implicit time integration and reached the same levels of discrepancy.

The control of maximum and minimum temperature in the channel (not presented) gave the same trend for the $C4$ convection scheme. In fact, no real improvement is obtained concerning the regulation of temperature extrema when time integration is implicit.

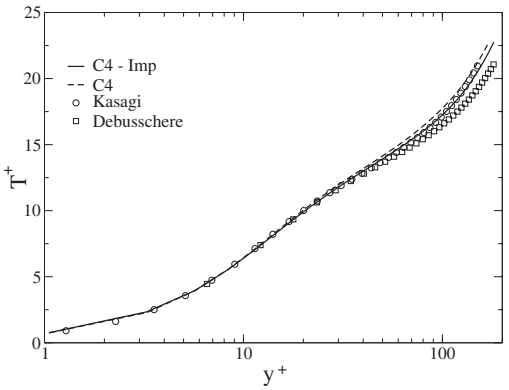

Figure 23. Distribution of mean resolved temperature in wall co-ordinates.

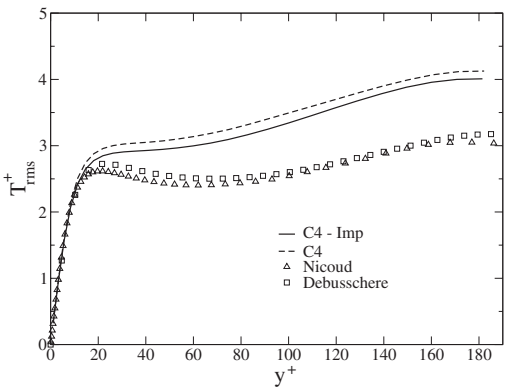

Figure 24. Distribution of resolved temperature fluctuations in wall co-ordinates.

4.3.3. Effect of the SGS model. Using a diffusive scheme may lead to recommend a total suppression of SGS modelling as reported in some MILES approaches [1, 2].

The present section is to measure the role played by the SGS model. In this section, results obtained with the $C4$, $Q3$ with and without SGS model on the temperature equation are reported (see Table III).

We see in Figures 25 and 26 that the sub-grid scale model has a very slight positive effect on the results even in conjunction with a regularizing scheme such as the $Q3$ scheme. Mean temperature profiles show little dependence on the use of a SGS model. Fluctuations in the case of the $Q3$ scheme without model are slightly under-estimated, especially in the vicinity of the wall. Fluctuations given by the $C4$ scheme without model are subject to the inverse behaviour as the $Q3$ scheme since fluctuations are higher in the $C4 - noMod$ case than in the $C4$ case.

For the present resolution, the use of a sub-grid scale model does not significantly improve the results.

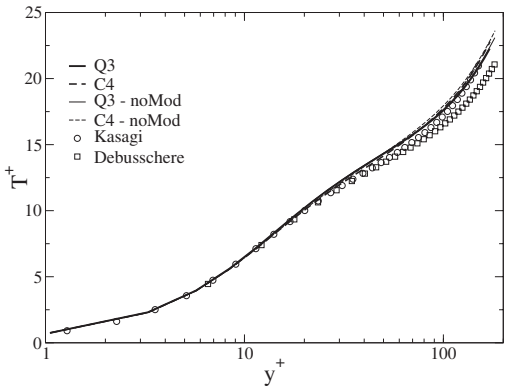

Figure 25. Distribution of resolved temperature fluctuations in wall co-ordinates.

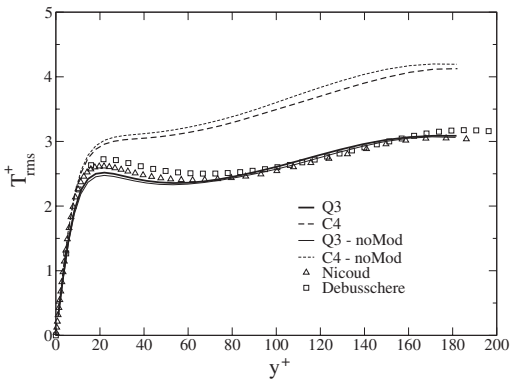

Figure 26. Distribution of resolved temperature fluctuations in wall co-ordinates.

5. INTERPRETATIONS

The purposes of this section are dual:

(i) To propose an explanation concerning the observed effects and the sensitivity of the results regarding the convection scheme;
(ii) To analyse the use of the *Q*3 scheme for the temperature field and propose future works.

If one considers the numerical resolution of the incompressible Navier–Stokes equation, we are confronted to two constraints. The first one is by the zero divergence constraint coming along with the Poisson equation applying on the pressure, which can limit possible too large velocity fluctuations by reorganizing the energy through all three velocity components.

The second one concerns the SGS model itself: the expression of majority of the sub-grid-scale models shows a direct relation between the velocity field and the value of the eddy viscosity, thus resulting in a strong coupling between the resolved field and the turbulent

viscosity. Given that, if a region shows large velocity gradients, eddy-viscosity will participate to the natural damping of velocity and stabilize the flow.

For these reasons, centred schemes are well suited for momentum. Moreover it is known that the use of centred schemes provide better results concerning the friction coefficients (an attempt of using the $Q3$ scheme for the convection term in the momentum equation showed a poor behaviour: the friction coefficient drops down to much smaller values than with a centred scheme).

On the contrary, the SGS heat flux model we use is only related to the velocity field and not only to the temperature gradients, leading to a decoupling between temperature field and turbulent heat diffusion. If one considers the case where the velocity field is smooth enough but the temperature field is perturbed, no turbulent diffusion will damp these temperature fluctuations since it will be directly related to the eddy viscosity.

Therefore, no stabilizing effect is achieved neither by the SGS modelling effect, nor by the use of a conservative scheme. Whereas the use of a high order regularizing type scheme helps controlling the production of spurious oscillations.

The use of $Q3$ scheme for temperature and centred scheme for momentum may therefore appear as a good compromise.

Two drawbacks have been identified: (i) the temperature field is homogenized faster by using the $Q3$ than $C4$ scheme; (ii) and fluctuations of temperature field may appear as a little damped when compared to equivalent DNS (see Figure 19).

The first point is of little importance regarding industrial applications.

The second point and the examination of Figure 19 leads to the conclusion that centred schemes help recovering the peak intensity of fluctuations in the near wall region whereas only regularizing scheme may provide a 'good' shape of temperature fluctuation for the fully turbulent region. This statement gives ride to two comments:

(i) First it comes along with a common practice of external aerodynamic people which may prefer centred schemes and suppress numerical damping in the near wall region [34];
(ii) Second, it suggests a shape of optimized scheme for the present configuration as follows:

$$\boldsymbol{\nabla}.(\mathbf{U}T) = (f)\boldsymbol{\nabla}.(\mathbf{U}T)_{Q3} + (1-f)\boldsymbol{\nabla}.(\mathbf{U}T)_{C4} \tag{10}$$

f being a function between 0 and 1. The underlying philosophy being that $f \simeq 0$ is limited to areas where molecular diffusion dominates, whereas $f \simeq 1$ in other places.

Such a numerical scheme has not been tested in the present study but may be part of forthcoming work.

However, present results obtained with the $Q3$ scheme for the temperature field suggest to recommend its use for LES involving temperature transport, even in the case of wall bounded flows.

6. CONCLUSIONS

Large eddy simulations of temperature transport have been done for several configurations including a two dimensional Tee junction, the isotropic turbulence decay of a passive scalar and the periodic channel flow with heat transfer to study the effects of the convection schemes in the discretized temperature equation.

Attention was payed to the capability of different classical convection schemes (Centred fourth order, Upwind first order and Quick third order) to respect some physical criteria, such as temperature variance conservation and respect of the physical bounds imposed by the physical problem.

Centred type schemes showed their limits in all configurations calculated here: temperature physical bounds are not respected due to spurious numerical instabilities leading in part to an over-estimation of temperature fluctuations in the channel flow configuration for example. But still, centred schemes reproduce correctly energy decay and do not damp the small temperature scales as seen in the isotropic turbulence.

Upwind type schemes gave physical results between imposed physical bounds in all investigated cases, but exhibited damping effects. These effects lead to discard the first order Upwind scheme for which temperature fluctuations are highly under-predicted in all situations.

The Quick scheme revealed to be a good compromise between numerical stability, variance conservation and damping effect on temperature fluctuations.

In the present channel flow configuration the role of the sub-grid scale model was not clearly shown since space discretization was accurate: in the well resolved LES framework it seems that the only use of an adequate convection scheme (such as a third order quick scheme with limiter) enables to recover proper turbulence dynamics, and therefore fluctuations, for the scalar transport.

APPENDIX A: DESCRIPTION OF THE GRID ARRANGEMENT AND THE CONVECTION SCHEMES

We briefly introduce the numerical convection schemes used in this work.

The computational grid is a staggered grid where velocities are located at the face centre and temperature is discretized at the centre of the elements, as shown in Figure A1.

The integration on the control volume around temperature points derives the following equations, using the Ostrogradsky theorem:

$$\iiint_{\Omega} \frac{\partial}{\partial x_i}(TU_i)\,\mathrm{d}\Omega = \oint_{\partial\Omega} TU_i.n_i\,\mathrm{d}S = \sum_{e=1}^{2N_{\mathrm{dim}}} T_e U_e S_e \tag{A1}$$

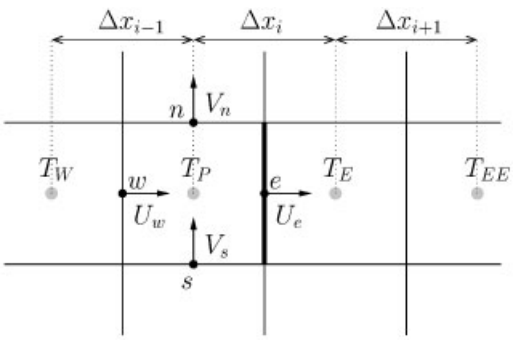

Figure A1. Grid arrangement (and conventions) on the staggered grid.

where T_e is the interpolated value of the scalar at the face to calculate the flux, S_e is the face surface and U_e is the transport velocity at the face e.

Convection schemes try to give an approximation of the interpolated value T_e.

A.1. First order upwind scheme ($U1$)

Using the upstream point value to approximate the temperature at point e is equivalent to using a backward (or forward, depending on the flow direction) difference approximation for the first derivative.

Thus, this simple upwind differencing scheme method is the following:

$$T_e = \begin{cases} T_{\mathrm{P}} \text{ if } (U_e.n_e) > 0 \\ \\ T_{\mathrm{E}} \text{ if } (U_e.n_e) < 0 \end{cases} \tag{A2}$$

This scheme is of first order and is numerically diffusive: its truncation error resembles a diffusive flux in $\partial T/\partial x$. However, it is unconditionally stable but induces large diffusive effects (see Reference [35]).

A.2. Third order quick scheme ($Q3$)

The QUICK scheme (for quadratic upwind interpolation for convective kinetics) (see Reference [36]) is still an upwind scheme as the previous one. It is much more complex but has a substantial higher order since it consists of a quadratic interpolation on three points: 2 upwind points and 1 downwind point.

The interpolation combines a linear interpolation of the two nearest points of the flux face, and a curvature term defined with upstream and downstream points.

The interpolated temperature at e is then defined as

$$T_e = \frac{1}{2}(T_{\mathrm{P}} + T_{\mathrm{E}}) - \frac{1}{8}\Delta x_i^2 \mathrm{CURV} \tag{A3}$$

$$\begin{aligned} \text{if } (U_e.n_e) > 0 : \mathrm{CURV} &= \frac{1}{\Delta x_{i-1}}\left[\frac{T_{\mathrm{E}} - T_{\mathrm{P}}}{\Delta x_i} - \frac{T_{\mathrm{P}} - T_{\mathrm{W}}}{\Delta x_{i-1}}\right] \\ \text{if } (U_e.n_e) < 0 : \mathrm{CURV} &= \frac{1}{\Delta x_i}\left[\frac{T_{\mathrm{EE}} - T_{\mathrm{E}}}{\Delta x_{i+1}} - \frac{T_{\mathrm{E}} - T_{\mathrm{P}}}{\Delta x_i}\right] \end{aligned} \tag{A4}$$

This algorithm can show numerical oscillations, a limiter is then used to eliminate them. In the case of scalar transport, the FRAM limiter is usually used (see Reference [37]).

A.3. Fourth order centered scheme ($C4$)

The fourth order Centred scheme for non-uniform grids reaches a somewhat high complexity and reads as

$$T_e = g_1 T_{\mathrm{W}} + g_2 T_{\mathrm{P}} + g_3 T_{\mathrm{E}} + g_4 T_{\mathrm{EE}} \tag{A5}$$

where the four coefficients are defined by

$$
\begin{aligned}
g_1 &= \frac{-\Delta x_i^2((\Delta x_i/2)+\Delta x_{i+1})}{4(\Delta x_{i-1}+\Delta x_i+\Delta x_{i+1})(\Delta x_i+\Delta x_{i-1})\Delta x_{i-1}} \\
g_2 &= \frac{(\Delta x_i+2\Delta x_{i+1})(\Delta x_i+2\Delta x_{i-1})}{8(\Delta x_i+\Delta x_{i+1})\Delta x_{i-1}} \\
g_3 &= \frac{(\Delta x_i+2\Delta x_{i+1})(\Delta x_i+2\Delta x_{i-1})}{8(\Delta x_i+\Delta x_{i-1})\Delta x_{i+1}} \\
g_4 &= \frac{-\Delta x_i^2((\Delta x_i/2)+\Delta x_{i-1})}{4(\Delta x_{i-1}+\Delta x_i+\Delta x_{i+1})(\Delta x_i+\Delta x_{i+1})\Delta x_{i+1}}
\end{aligned}
\tag{A6}
$$

ACKNOWLEDGEMENTS

The authors thank the referees for their insightful comments. They also gratefully acknowledge Prof. F. Nicoud and B. Debusschere for their collaboration by making their DNS data available for this work.

REFERENCES

1. Oran ES, Boris JP. Computing turbulent shear flows—a convenient conspiracy. *Computers in Physics* 1993; **7**(5):523.
2. Fureby C, Grinstein FF. Monotically Integrated Large-eddy Simulation of free shear flows. *AIAA Journal* 1999; **37**(5):544–556.
3. Morinishi Y, Lund TS, Vasilyev OV, Moin P. Fully conservative higher order finite difference schemes for incompressible flow. *Journal of Computational Physics* 1998; **143**:90–124.
4. Mittal R, Moin P. Suitability of upwind-biased finite difference schemes for large-eddy simulation of turbulent flows. *AIAA Journal* 1997; **35**(8):1415–1417.
5. Garnier E, Mossi M, Sagaut P, Comte P, Deville M. On the use of shock-capturing schemes for LES. *Journal of Computational Physics* 1999; **153**:273–311.
6. Ducros F, Ferrand V, Nicoud F, Weber C, Darracq D, Gacherieu C, Poinsot, T. LES of the Shock/Turbulence Interaction. *Journal of Computational Physics* 1999; **152**:517–549.
7. Kong H, Choi H, Lee JS. Direct numerical simulation of turbulent thermal boundary layers. *Physics of Fluids* 2000; **12**(10):2555–2568.
8. Kong H, Choi H, Lee JS. Dissimilarity between the velocity and temperature fields in a perturbed turbulent thermal boundary layer. *Physics of Fluids* 2001; **13**(5):1466–1479.
9. Akselvoll K, Moin P. Large-eddy simulation of turbulent confined coannular jet. *Journal of Fluid Mechanics* 1996; **315**:387–411.
10. Montreuil E, Sagaut P, Labbé O. Assessment of non-Fickian sub-grid-scale models for passive scalar in a channel flow. In *Workshop on Direct and Large Eddy Simulation*, Isaac Newton Institute for Mathematical Sciences, Cambridge, May 1999.
11. Kim J, Moin P. Transport of passive scalars in a turbulent channel flow. In *Proceedings of the 6th Symposium on Turbulent Shear Flows*, September 1987.
12. Lyons SL, Hanratty TJ, McLaughlin JB. Direct numerical simulation of passive heat transfer in a turbulent channel flow. *International Journal of Heat Mass Transfer* 1991; **34**(4/5):1149–1161.
13. Kawamura H, Abe H, Shingai K. DNS of turbulence and heat transport in a channel flow with different Reynolds and Prandtl numbers and boundary conditions. In *3rd International Symposium on Turbulence*, *Heat and Mass Transfer* 2000; 15–32.
14. Kasagi N, Tomita Y, Kuroda A. DNS of passive scalar field in a turbulent channel flow. *Journal of Heat Transfer* 1992; **114**:598–606.
15. Nicoud F, Poinsot T. DNS of a channel flow with variable properties. *Turbulence and Shear Flow Phenomena* 1, 1999; 697–702.
16. Nicoud F. Numerical study of a channel flow with variable properties. *Center for Turbulent Research*, *Annual Research Briefs*, 1998; 289–310.

17. Wang W-P, Pletcher RH. On the large eddy simulation of a turbulent channel flow with significant heat transfer. *Physics of Fluids* 1996; **8**(12):3354–3366.
18. Lee JS, Pletcher H. LES of a turbulent channel flow with buoyancy effects. *AIAA Journal* 2001; **2001**(0431).
19. Peng S-H, Davidson L. On a sub-grid-scale heat flux model for large eddy simulation of turbulent thermal flow. *International Journal of Heat Mass Transfer* 2002; **45**:1393–1405.
20. Leonard A. Energy cascade in large-eddy simulations of turbulent fluid flows. *Advances in Geophysics* 1974; **18A**:237–248.
21. Lesieur M, Métais O. New trends in large-eddy simulations of turbulence. *Annual Reviews of Fluid Mechanics* 1996; **28**:45–85.
22. Sagaut P. *Large-Eddy Simulation for Incompressible Flows*. Springer Verlag: Berlin, 2002.
23. Lesieur M. *Turbulence in Fluids*. Kluwer Academic Publishers: Dordrecht, 1997.
24. Nicoud F, Ducros F. Sub-grid-scale stress modelling based on the square of the velocity gradient tensor. *Flow, Turbulence and Combustion* 1999; **62**:183–200.
25. Calvin C, Cueto O, Emonot P. An object-oriented approach to the design of fluid mechanics software. *Mathematical Modeling and Numerical Analysis* 2002; M2AN 2002, special issue.
26. Williamson JH. Low storage Runge–Kutta schemes. *Journal of Computational Physics* 1980; **35**:48–56.
27. Métais O, Lesieur M. Spectral large-eddy simulation of isotropic and stably stratified turbulence. *Journal of Fluid Mechanics* 1992; **239**:157–194.
28. Dean RB. Reynolds number dependence of skin friction and other bulk flow variables in two-dimensional rectangular duct flow. *Journal of Fluids Engineering—Transaction of the ASME* 1978; **100**:215–223.
29. Rollet-Miet P. Simulation des Grandes Echelles sur maillages non-structurés pour géométries complexes. *Ph.D. Thesis*, Ecole Centrale de Lyon, 1997.
30. Kim J, Moin P, Moser R. Turbulence statistics in fully developed channel flow at low Reynolds number. *Journal of Fluid Mechanics* 1987; **177**:133–166.
31. Kasagi N, Iida O. Progress in direct numerical simulation of turbulent heat transfer. In *Proceedings of the 5th ASME/JSME Joint Thermal Engineering Conference*, 1999.
32. Debusschere B, Rutland CJ. Turbulent scalar transport mechanisms in plane channel and couette flows. *Private communication*, *International Journal of Heat and Mass Transfer*, August 2002, submitted.
33. Kays WM, Crawford ME. *Convective Heat and Mass Transfer*. McGraw-Hill: New-York, 1980.
34. Swanson R-C, Turkel E. On central-difference and upwind schemes. *Journal of Computational Physics* 1992; **101**:292.
35. Ferziger JH, Peric M. *Computational Methods for Fluid Dynamics*. Berlin: Springer, 1997.
36. Leonard BP. Simple high-accuracy resolution program for convective modelling of discontinuities. *International Journal for Numerical Methods in Fluids* 1988; **8**:1291–1318.
37. Chapman M. FRAM—Nonlinear damping algorithms for the continuity equation. *Journal of Computational Physics* 1981; **44**:84–103.

